Tensile Stress in a Porous Medium Due to Gas Expansion

Nieck E. Benes, P. Maarten Biesheuvel, and Henk Verweij
Laboratory of Inorganic Materials Science, Dept. of Chemical Technology, University of Twente, P.O. Box 217, 7500 AE Enschede, The Netherlands

Stress profiles develop in a porous material due to a gas-phase pressure difference and subsequent gas flow. If stresses become tensile, material failure (explosion and blistering) can occur. Stress profiles are calculated for an asymmetric inorganic porous disk-like membrane material placed in a pressure vessel, which is depressurized. The stress that develops in the membrane material depends on the gas-phase pressure and the porosity. The gas-phase pressure is a function of place, time and characteristics of the membrane, the vessel and the valve. Two regimes are identified for membrane depressurization, and a critical initial pressure is defined below which tensile stresses cannot develop. The theory presented combines the dusty gas model with balances for mass, momentum, and mechanical energy.

Introduction

The endurance of a membrane material is crucial for use under harsh conditions in industrial separation processes or membrane reactors (Saracco et al., 1994), and is often tested in a pressure vessel with elevated pressure and temperature with gas-phase composition simulating true process conditions. The membrane is simply placed on a grid within this vessel (see Figure 1). In a similar experiment, the gas-phase adsorption is measured to estimate to which extent surface diffusion occurs. After the experiment, a valve is opened to depressurize the vessel.

The membranes used in our laboratories consist of a thin mesoporous γ-alumina layer with separation characteristics (typical pore size 2–5 nm and thickness 4 μm) on top of a macroporous α-alumina support layer (pore size 80 nm and thickness 2 mm), which gives strength to the membrane (see Table 1 for the relevant material properties). After testing these membranes under steam reforming conditions at an elevated temperature, elevated pressure, and subsequent depressurization, the γ-layers had blistered on several occasions (see Figure 2), whereas this did not occur in other gas atmospheres.

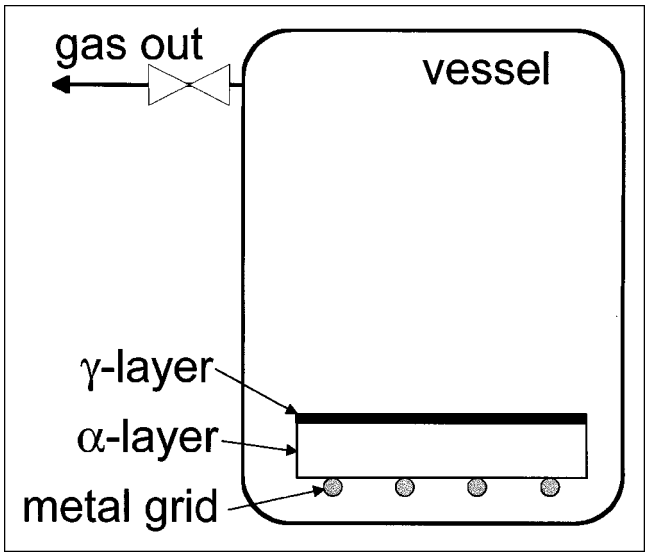

Figure 1. Geometry of depressurization experiment.

The cause of failure is the lowering of the γ-layer cohesion strength or the adhesion strength of the γ-layer on the α-layer due to a reaction with one of the gas-phase components in

Correspondence concerning this article should be addressed to N. E. Benes.

Table 1. Data Used in Simulations (Base Case)

p_0	initial pressure	30×10^5	Pa
V_{ves}	volume vessel	10^{-3}	m^3
T	temperature	873	K
μ	viscosity	3.74×10^{-3}	$Pa\cdot s$
M	mole weight CO_2	44×10^{-3}	$kg\cdot mol^{-1}$
ρ_α	density alumina	4×10^3	$kg\cdot m^{-3}$
L_α	thickness α layer	2×10^{-3}	m
ϵ_α	porosity α layer	0.30	
τ_α	tortuosity α layer	1	
$r_{p,\alpha}$	pore radius α layer	80×10^{-9}	m
L_γ	thickness γ layer	4×10^{-6}	m
ϵ_γ	porosity γ layer	0.30	
τ_γ	tortuosity γ layer	1	
$r_{p,\gamma}$	pore radius γ layer	1.25×10^{-9}	m

combination with a tensile stress that develops in the material during depressurization. To estimate the decrease of the cohesion or adhesion strength, a model is set up that describes stress profiles developing during depressurization as a function of the relevant material properties and operating conditions. In the model the following issues are addressed:

- First, the mass balance over the vessel is solved implementing an expression for flow through the valve based on the steady-state macroscopic mechanical energy balance or Bernoulli equation. In the latter, friction in the valve is implemented using a so-called friction loss factor e_v;
- Secondly, the gas-phase pressure profile developing in the membrane is calculated implementing the dusty gas model; and
- Thirdly, compressive and tensile stresses within the membrane in the direction of flow are calculated applying the steady-state momentum balance.

The theory as presented in this article can be adjusted to describe several related problems in chemical engineering, such as:

(1) *The production of popcorn* (Da Silva et al., 1993). In this process, heat is supplied to the corn resulting in water evaporation inside the kernel and subsequent pressure buildup. When the tensile stress in the so-called pericarp exceeds the strength, the corn pops. Here, the stress that develops is primarily parallel to the toplayer surface, contrary to the membrane case.

(2) *The production of polymer* by heterogeneous catalysis, such as polypropylene over a Ziegler-Natta catalyst. Due to polymer formation, a tensile stress develops within the particle and catalyst fragmentation occurs. If this fragmentation is uncontrolled, a polymer with inferior properties can result (Ferrero and Chiovetta, 1987; Niegisch et al., 1994). Here, failure of the rigid catalyst particle is caused by the development of a second solid phase and not by a gas-phase pressure difference.

(3) An example of a nonrigid structure that deforms under the influence of pressure gradients is found in the description of cake formation from a suspension or slurry as in gravity settling (Buscall, 1990), centrifugal sedimentation, or centrifugal filtration (Sambuichi et al., 1987; Tiller and Hsyung, 1993). Here, the porous medium is often considered as a collapsing structure that densifies irreversibly due to compressive stresses.

(4) *Coating of piping* in process industry. Pipelines are often protected from possible corrosion by the aggressive components in a gas-stream by the application of a coating. It is a common problem that inferior coatings blister off from the pipe wall when the system is depressurized. During operation at high pressures (such as up to hundreds of bars in gas transfer), gas diffuses into the coating. During depressurization, the pressure inside the coating remains higher, creating a tensile stress and possible subsequent blistering (Davis and Thompson, 1994). The only difference with the membrane case is the fact that in the coating, gas can only flow out on one side.

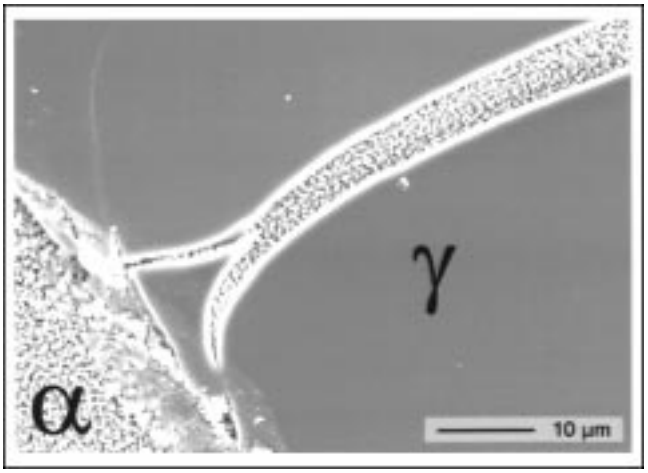

Figure 2. Asymmetric inorganic membrane employed under steam reforming conditions.

Speckled areas: substrate (α alumina); dark areas: γ alumina layer which clearly blistered off.

Theoretical Background

A model is presented to describe the stress that develops in a porous asymmetric membrane, consisting of a γ-layer on top of an α-layer. The membrane is placed in a closed vessel at an initial pressure p_0 (see Figure 1). At time $t = 0$ s, a valve is opened after which the pressure in the vessel decreases with time. It is assumed that

- The ideal gas law can be applied.
- The gas phase consists of one component.
- The structural properties of the membrane are independent of stress.
- The pressure and temperature in the vessel are homogeneous.
- The viscosity of the gas is independent of pressure.
- In the membrane, only transport in the direction perpendicular to the α/γ-interface is of importance and the pressure distribution perpendicular to the direction of flow is uniform.
- Stress in the direction of flow causes failure. A stress that could develop parallel to the surface, as in popcorn popping, is neglected, because the membrane lies freely upon the grid (see Figure 1) and is not clamped on its outer perimeter. The difference between these forms of stress is also noted by Strawbridge and Evans (1995), who describe ''through-thickness cracking'' and ''cracking along the coating substrate interface.''

In order to estimate the stress in the membrane, it is necessary to describe the change in pressure in the vessel and the mass transport phenomena inside the membrane. Consequently, the pressure profiles inside the porous medium have to be related to stress in the material.

Pressure change in the vessel

The pressure change in the vessel can be calculated from a mass balance. If the volume of the membrane is small compared to that of the vessel, this equation becomes

$$\frac{V_{\text{ves}} M}{R} \frac{\partial}{\partial t}\left(\frac{p}{T}\right) = -\phi_{m,\text{out}} \tag{1}$$

where V_{ves} is the volume of the vessel (m^3), M is the mole weight of the gaseous component ($kg \cdot mol^{-1}$), R is the gas constant (8.3144 $J \cdot mol^{-1} \cdot K^{-1}$), T is the temperature (K), p is the pressure (Pa), and $\phi_{m,\text{out}}$ is the mass flow out of the vessel ($kg \cdot s^{-1}$).

The change of temperature in time of the gas in the vessel can be calculated from the following energy balance (for instance, Westerterp et al., 1984, Eq. VI.1)

$$V_{\text{ves}}\left(\frac{\partial(\rho u)}{\partial t}\right) = -\phi_{m,\text{out}} h + UA(T_{\text{air}} - T) \tag{2}$$

where ρ is the density of the gas ($kg \cdot m^{-3}$), U is the overall heat-transfer coefficient ($J \cdot m^{-2} \cdot K^{-1} \cdot s^{-1}$), u and h, respectively, are the internal energy and enthalpy of the gas ($J \cdot kg^{-1}$), and A is the heat exchange surface (m^2). It becomes clear from Eq. 2 that a temperature change may occur during depressurization (see Xia et al., 1993, Eq. 28). However, in this study the temperature change is neglected for reasons of simplicity.

For a quasi-stationary situation, an expression for the mass flow out of the vessel can be obtained from the extended Bernoulli equation or steady-state macroscopic mechanical energy balance over the valve. For an isothermal system containing a compressible fluid, the mechanical energy balance over the valve is (Bird et al., 1960, Eq. 7.3-2)

$$\Delta\frac{1}{2}\frac{\langle \bar{v}^3 \rangle}{\langle \bar{v} \rangle} + \Delta\hat{\Phi} + \int_{p_1}^{p_2}\frac{1}{\rho}dp + \hat{W} + \hat{E}_v = 0 \tag{3}$$

where $\hat{\Phi}$ is the potential energy ($J \cdot kg^{-1}$), $\hat{W}$ the rate at which the systems performs mechanical work on its surroundings ($J \cdot kg^{-1}$), and $\hat{E}_v$ is the "friction loss," that is, the rate at which mechanical work is irreversibly converted to thermal energy ($J \cdot kg^{-1}$).

Due to the high flow rates through the valve, the Reynolds number *Re* will be large and the flow will be turbulent. For turbulent flow through the valve, the velocity profile can be assumed flat; thus, the ratio $\langle \bar{v}^3 \rangle / \langle \bar{v} \rangle$ can be replaced by $\langle \bar{v} \rangle^2$. From now on, the horizontal bar above the velocity v will be omitted as well as the $\langle\ \rangle$-sign. The gas flows in horizontal direction, so the term $\Delta\hat{\Phi}$ can be discarded. Because no mechanical work is exerted by the gas, the term $\hat{W}$ can be discarded as well. The friction loss $\hat{E}_v$ is correlated to the friction loss factor e_v by (Bird et al., 1960, Eq. 7.4-5)

$$\hat{E}_v = \frac{1}{2}v^2 e_v \tag{4}$$

The value of e_v depends upon the type of valve used and can be found in, for instance, Bird et al. (1960, Table 7.4-1) or Perry and Green (1984, Table 5-14). A typical value is $e_v =$ 6–10 for a globe valve. A differential form of Eq. 3 is used, because velocity v is not constant within the valve

$$d(v^2) + \frac{1}{\rho}dp + \frac{1}{2}v^2 e_v = 0 \tag{5}$$

Mass flow ϕ_m and velocity v are related by

$$\phi_m = v \cdot A \cdot \rho \tag{6}$$

with A the open area of the valve (m^2). Substitution of Eq. 6 in Eq. 5 and subsequent integration, with as integration limits the pressure inside the vessel p and the atmospheric pressure outside of the vessel p_{atm} leads to the following expression for the mass flow

$$\phi_m = A\sqrt{\frac{M}{RT}\frac{(p^2 - p_{\text{atm}}^2)}{[2\ln(p/p_{\text{atm}}) + e_v]}} \tag{7}$$

Mass transport in the porous medium

Inside the porous membrane, the pressure can be calculated from the following equation of continuity of mass

$$\frac{\epsilon_i}{RT}\left(\frac{\partial p}{\partial t}\right) = -\left(\frac{\partial N}{\partial x}\right) \tag{8}$$

The subscript i either denotes the α- or γ-layer, N ($mol \cdot m^{-2} \cdot s^{-1}$) denotes the molar flux, and ϵ denotes the porosity. For macroporous and mesoporous media, it is generally accepted (Krishna, 1987) that gas transport can be satisfactorily described with the dusty gas model (Mason and Malinauskas, 1983), which gives expressions for the molar fluxes of components present in the membrane. The flux expression obtained from the dusty gas model is in the case of one component

$$N = -\left(D_{Kn} + \frac{B_0}{\mu}p\right)\left(\frac{1}{RT}\frac{\partial p}{\partial x}\right) \tag{9}$$

This expression contains the effective Knudsen diffusion coefficient

$$D_{Kn} = \frac{4}{3}K_0\sqrt{\frac{8RT}{\pi M}} \tag{10}$$

The parameters K_0 and B_0 depend only on the structure of the porous medium and can be obtained from experiment. According to Mason and Malinauskas (1983), these can be

calculated directly from the tortuosity τ and the pore radius r_p (m)

$$K_0 = \left(\frac{\epsilon r_p}{2\tau} \right)_i \tag{11}$$

$$B_0 = \left(\frac{\epsilon r_p^2}{8\tau} \right)_i \tag{12}$$

Relation between pressure and stress in a porous medium

From the gas-phase pressure profile within the membrane, the stress profile can be calculated using the steady-state momentum balance (Bird et al., 1960, Eq. 7.2-3)

$$F = -\Delta\left(\frac{\langle \bar{v}^2 \rangle}{\langle \bar{v} \rangle} w + p \cdot A_g \right) + m_{\text{tot}} \cdot g \tag{13}$$

For a flat velocity profile $\langle \bar{v}^2 \rangle / \langle \bar{v} \rangle$ can be replaced by $\langle \bar{v} \rangle$ after which the horizontal bar and the $\langle\,\rangle$-sign are again omitted. The mass-flow w is given by $w = A_g \cdot \rho \cdot v$ and the surface perpendicular to flow is given by A_g. For a disk with a diameter of 3.6 cm and a porosity of $\epsilon = 0.3$, the maximum value for the momentum flow $A_g \cdot \rho \cdot v \cdot v$ for the base case of our simulation is 0.13 N at the outside of the α-layer. A typical value of $p \cdot A_g$ in the experiment would be 900 N. The weight of the disk is roughly given by 0.05 N. Therefore, all terms except for the pressure term are discarded.

A gas-phase pressure differential will lead to gas flow through the material and friction forces on the pore walls. These forces are now given by the simplified form of Eq. 13 (see Evans III et al., 1962, Eq. 4).

$$F = -\Delta(p \cdot A_{g,i}) \tag{14}$$

The force exerted by the solid structure is similarly given by the sum of stress σ and solid surface $A_{s,i}$

$$F = -\Delta(\sigma \cdot A_{s,i}) \tag{15}$$

For an isotropic material, the cross-sectional surface area of both the gas and solid phase are related to the porosity ϵ_i by

$$\frac{A_{g,i}}{A_{\text{tot}}} = \epsilon_i; \qquad \frac{A_{s,i}}{A_{\text{tot}}} = 1 - \epsilon_i \tag{16}$$

After setting the sum of Eqs. 14 and 15 equal to zero and implementation of Eq. 16, again assuming a constant porosity ϵ_i, we arrive at

$$\epsilon_i \Delta p + (1 - \epsilon_i)\Delta\sigma = 0 \tag{17}$$

Rewriting Eq. 17 with $\Delta p = p_i(x) - p_{\text{ves}}$ and $\Delta\sigma = \sigma_i(x) - p_{\text{ves}}$ results in

$$\sigma_i(x) = p_{\text{ves}} - \frac{\epsilon_i}{1 - \epsilon_i}\{ p_i(x) - p_{\text{ves}}\} \tag{18}$$

At the outside of the membrane, compressive stresses remain present while tensile stresses can develop within the membrane. Only if the porosities of both layers are equal, the value of the stress is continuous at the α/γ-interface; if not, a step change in stress occurs.

Results and Discussion

Numerical scheme

After substitution of Eq. 7 in Eq. 1, a nonlinear differential equation is obtained for the pressure change in the vessel, which is solved with a fourth-order Runge-Kutta method (Atkinson, 1989). Gas transport inside the membrane is described by Eq. 8, which is an instationary, nonlinear, second-order, parabolic, and partial differential equation. Because analytical solutions for this type of equation are not readily found, one has to resort to numerical methods. After time transformation, the equation is discretized. The resulting set of nonlinear equations is solved with a Newton-Raphson iteration procedure and the numerical scheme is implemented in Borland Delphi code (a complete derivation of the numerical scheme and a copy of the program are available at the internet site: http://www.ct.utwente.nl/~ims/).

Simulations have been carried out for the base case as defined by the data presented in Table 1. These data correspond to CO_2 depressurization of a typical asymmetric porous membrane, as used in our laboratory. Subsequently, results will be presented for the pressure change in the vessel, the pressure development inside the membrane, and the stress in the membrane material.

Pressure in the vessel

In Figure 3 the pressure in a vessel of 10^{-3} m^3 is shown for different values of A and e_v as a function of time. Both A and e_v are changed over the same order of magnitude. The influence of A on the pressure profile is most eminent: if the open area A is increased, the curves shift to the right. The time of complete depressurization appears to depend linearly on the valve surface area A, as can be expected from Eq. 7

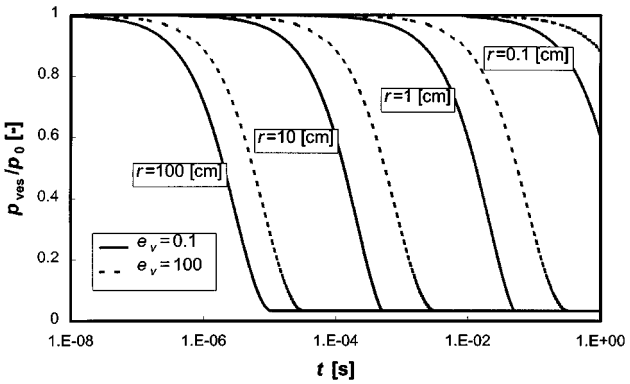

Figure 3. Pressure in a vessel of 10^{-3} m^3 as a function of time and valve geometry for different valve characteristics e_v and A ($= \pi r^2$) and an initial pressure of $p_0 = 30$ bar.

Base case calculation using the data presented in Table 1.

as well. For the friction loss factor e_v, only two extreme cases are presented, respectively, $e_v = 0.1$ and $e_v = 100$, corresponding to Perry and Green (1984, p. 5-38). For a smaller friction loss factor, the curves shift to the left. A high value of e_v results in a slightly slower approach of the atmospheric pressure.

With rapid depressurization, the system can no longer be considered isothermal, the quasi-stationary approach for the mechanical energy balance over the value no longer holds, and one has to resort to a more accurate description (see Xia et al., 1993). Such a refined model is beyond the scope of this study, and the error made is accepted for now.

Pressure inside the membrane

Due to mass-transfer limitations, pressure profiles will evolve inside the membrane. In Figure 4, typical pressure profiles in the membrane as a function of place and time are presented. The sharp change in pressure on the lefthand side of the figure denotes the pressure drop over the γ-layer, which appears to have a maximum at some point in time during the depressurization process. The moment at which this maximum is observed is strongly dependent on the rate of depressurization.

In Figure 5, the maximum pressure difference over the γ-layer during depressurization is presented as a function of the valve geometry. The pressure difference increases with valve surface area A, which is expected because the pressure in the vessel decreases faster for larger A and the mass transport limitations inside the membrane will then become more important. A smaller value of e_v enhances this effect and shifts the curves to the left.

It is possible to make a distinction between two regimes for the pressure difference over the γ-layer, depending on the time-scales of pressure decrease in the γ-layer and in the vessel (t_γ and t_v, respectively). For $t_\gamma < t_v$, the pressure in the γ-layer is able to follow the pressure decrease in the vessel. For $t_\gamma > t_v$, first, the pressure in the vessel decreases rapidly, after which the γ-layer depressurizes more slowly.

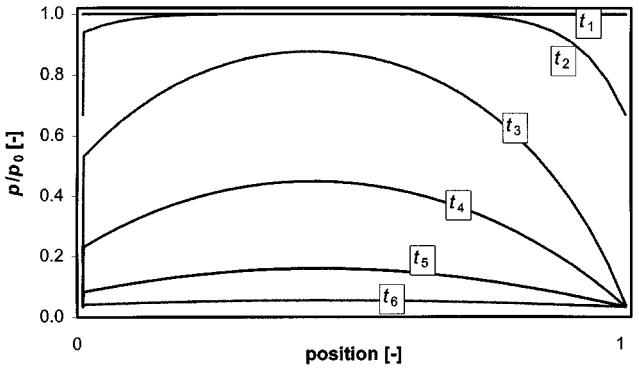

Figure 4. Pressure in the membrane as a function of position at increasing (arbitrary) t.

Position 0 is the outside of the γ-layer, while the outside of the α layer is located at position 1. The sharp change in pressure on the lefthand side of the graph indicates the thin γ-layer. Base case calculation using the data presented in Table 1, $A = 10^{-2}$ m^2 and $e_v = 10$.

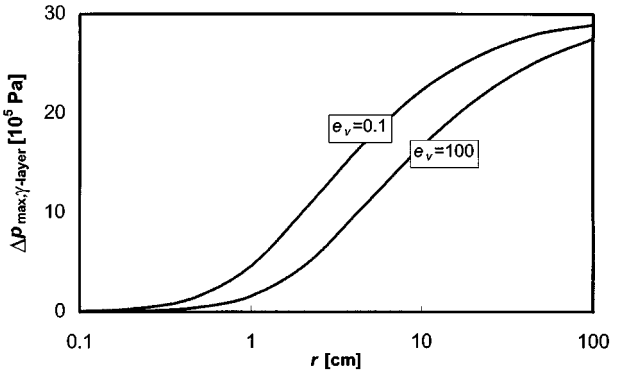

Figure 5. Maximum pressure difference over the γ layer during depressurization as function of valve geometry: e_v and $A = \pi r^2$.

Base case calculation using the data presented in Table 1.

In the first regime ($t_\gamma < t_v$), the pressure in the vessel decreases relatively slow and only a small driving force, that is, a pressure gradient, is needed to overcome the mass transport limitations present in the membrane. After a short period, the rate of change of pressure inside the membrane equals that of the vessel. At this moment, the maximum pressure difference is observed, because the curve of p_{ves} vs. time is concave. Here, the maximum pressure difference over the γ-layer is reached before the pressure in the vessel is atmospheric. This is contrary to the second regime ($t_\gamma > t_v$), where the maximum pressure difference over the γ-layer is determined by the time needed for p_{ves} to become atmospheric. If $t_\gamma \gg t_v$, an asymptotic pressure difference $p_0 - p_{atm}$ is observed, and not only at the α/γ-interface. The regimes coincide for $t_\gamma = t_v$, when the maximum pressure difference is found exactly when p_{ves} becomes atmospheric, which occurs at the transition or bending points in Figure 5. The existence of two regimes can be generalized for any location in the membrane.

Stress

The stress that develops in the material can either have a positive value (compressive stress) or a negative value (tensile stress). Especially when the stress becomes tensile, material failure (cracks, blistering, or explosion) may occur and, therefore, the maximum tensile stress, equivalent to the minimum stress, developing in the material is of special interest in this study.

In Figure 6 typical curves of the stress in the membrane as a function of position and time $\sigma(x,t)$ are presented. Initially, at t_1, $\sigma(x,t)$ is compressive and equal to the pressure in the vessel. At t_2, $\sigma(x,t)$ has decreased and becomes tensile ($\sigma < 0$) for the larger part of the membrane at t_3. After t_3, $\sigma(x,t)$ increases to atmospheric pressure in the entire membrane.

At any position x_i in the membrane, a minimum value for the stress $\sigma(x,t)$ will be observed at a certain point in time during the depressurization process. This minimum will be defined as $\sigma^{min}(x)$. A plot of $\sigma^{min}(x)$ closely resembles $\sigma(x,t_3)$ in Figure 6, but is not exactly similar: while $\sigma(x,t_3)$

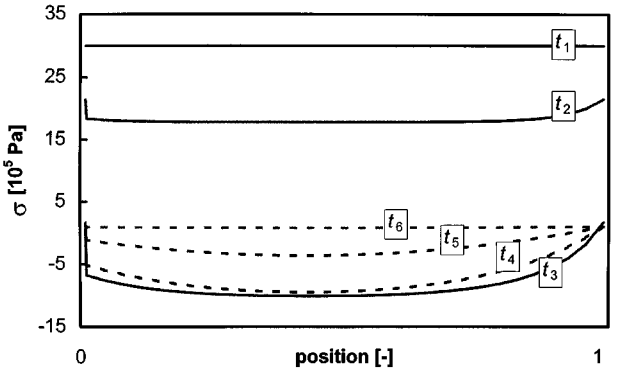

Figure 6. Stress as a function of position at increasing t.

Dotted lines: stress after minimum stress has been observed. Position 0 is the outside of the γ layer, while the outside of the α-layer is located at position 1. The sharp change in stress on the lefthand side of the graph indicates the thin γ layer. Base case calculation using the data presented in Table 1, $A = 10^{-2}$ m^2 and $e_v = 10$.

is a stress curve for time t_3, $\sigma^{\min}(x)$ contains points from different moments in time. Two points of $\sigma^{\min}(x)$ will be discussed in more detail, namely:

- $\sigma^{\min,\text{abs}}$: the minimum value of $\sigma^{\min}(x)$; and
- $\sigma^{\min,\text{int}}$: the value of $\sigma^{\min}(x)$ at the α/γ-interface.

In Figure 7, $\sigma^{\min,\text{abs}}$ and $\sigma^{\min,\text{int}}$ are presented as a function of valve geometry, that is, e_v and A. For small A, the stress $\sigma(x,t)$ remains compressive during the entire depressurization process, and $\sigma^{\min}(x)$ observed is approximately equal to the atmospheric pressure. The rate of mass transport in the membrane need not be very high, and pressure gradients in the membrane will thus be small. If A is increased, $\sigma^{\min}(x)$ decreases and at a certain A, $\sigma^{\min}(x)$ becomes tensile. On increasing A, first $\sigma^{\min,\text{abs}}$ starts to decrease. At larger A, $\sigma^{\min,\text{int}}$ starts to decrease as well. The sensitivity of $\sigma^{\min,\text{abs}}$ on changes in valve geometry is higher than for $\sigma^{\min,\text{int}}$, due to the additional resistance for mass transport between the position at which $\sigma^{\min,\text{abs}}$ is observed and the α/γ interface. A smaller friction loss factor e_v enhances the effect of increasing A, shifting the curves to the left.

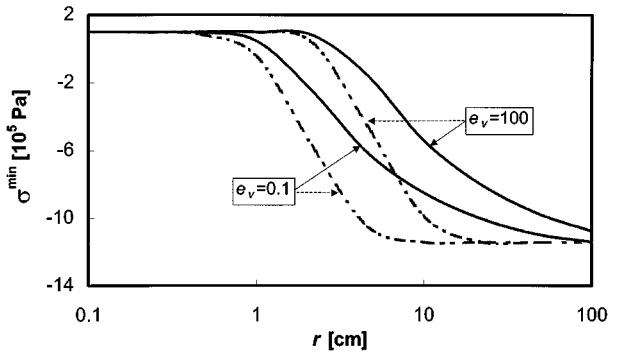

Figure 7. Minimum stress vs. valve geometry.

Dotted line denote $\sigma^{\min,\text{abs}}$; continuous lines denote $\sigma^{\min,\text{int}}$; base case calculation using the data presented in Table 1.

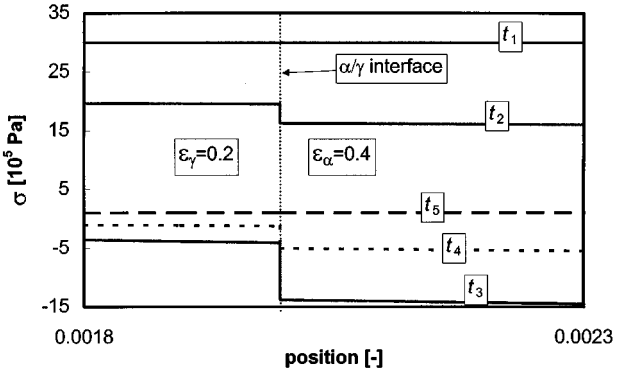

Figure 8. Discontinuity in stress at the α/γ interface for increasing t.

Base case calculation using the data presented in Table 1 except for the porosities.

For large enough A, the pressure in the vessel becomes atmospheric at a time-scale which is small compared to the time-scale of transport inside the membrane. As a result, the pressure inside the membrane is still almost uniform and close to p_0 when the vessel pressure has become atmospheric. In this situation $\sigma^{\min}(x)$ reaches an asymptotic value, which is only dependent on the porosity and can be calculated by substituting $p(x) = p_0$ and $p_{\text{ves}} = 1.013 \times 10^5$ Pa in Eq. 18 yielding $\sigma^{\min}(x) = -11.41 \times 10^5$ Pa for the base case simulations, using the data presented in Table 1.

Substitution of $\sigma = 0$ in Eq. 18 yields a simple expression for the minimum initial pressure p_0 necessary to introduce a tensile stress in the porous material

$$p_0 = \frac{p_{\text{atm}}}{\epsilon_i} \tag{19}$$

The porosities of both layers in Figures 6 and 7 have been chosen equal. In Figure 8 the stress in the vicinity of the α/γ-interface is presented for a membrane in which the porosities of both layers are not equal. Now, a discontinuity can be observed at the α/γ-interface with a higher stress at the layer with the lower porosity.

Perspectives

In the field of membrane and coating technology, the measurement of the interface adhesion strength of a toplayer on top of a substrate is of importance in numerous situations. A typical experiment is the Scotch tape test (Krongelb, 1968), in which Scotch-tape (Scotch Magic 810, 3M, St. Paul, MN) is stuck on the toplayer and drawn off with a certain force. If the contact tape-toplayer has the highest adhesion strength, the toplayer is pealed off from the substrate. If the tape comes off cleanly, the interface adhesion strength is higher. This experiment has a binary character: the interface adhesion strength is only compared with a certain standard, namely the tape-toplayer adhesion strength.

Based on the theory presented in this article, it is possible to determine more accurately the adhesion strength between two layers *of which at least one is porous*. To this end, the rate of pressure decrease in the vessel is increased in subsequent depressurization experiments until the toplayer peals off from the substrate. In case of a multilayered membrane, the sample can be placed in a gas permeation setup with the toplayer on the low-pressure side. Though the stress is compressive where the sealing touches the toplayer, it is tensile at some distance from the sealing and blistering can occur. By increasing the pressure difference over the membrane, and, thus, the tensile stress at the interface in subsequent experiments, the adhesion strength can be estimated using a simplification of the model presented in this article.

Conclusions

Due to internal mass transport limitations, pressure gradients evolve inside an asymmetric inorganic membrane placed in a vessel during depressurization. Dependent on the timescales of depressurization of both the vessel and the membrane, two regimes can be distinguished for the pressure change inside the membrane.

A tensile stress may evolve in the membrane when the initial pressure p_0 is larger than p_{atm}/ϵ_i and the pressure decrease in the vessel is fast enough. When the pressure in the vessel becomes atmospheric in an infinitely short time, the maximum possible tensile stress is observed, which only depends on porosity. If the porosities of the different layers of which the membrane exists are different, a discontinuity of the stress is observed at the interface between the layers.

The theory presented can be used to estimate the adhesion strength of a toplayer on top of a substrate, and can be adjusted to describe similar issues in chemical engineering.

Acknowledgments

The authors wish to thank ir. A. H. van den Boogaard of the faculty of mechanical engineering of the University of Twente for useful discussions during preparation of the manuscript.

Literature Cited

Atkinson, K. E., *An Introduction to Numerical Analysis*, 2nd ed., Wiley, New York (1989).

Bird, R. B., W. E. Stewart, and E. N. Lightfoot, *Transport Phenomena*, Wiley, New York (1960).

Buscall, R., ''The Sedimentation of Concentrated Colloidal Suspensions,'' *Colloids Surf*., **43**, 33 (1990).

Da Silva, W. J., B. C. Vidal, M. E. Q. Martins, H. Vargas, A. C. Pereira, M. Zerbetto, and L. C. M. Miranda, ''What Makes Popcorn Pop,'' *Nature* (*London*), **362**, 417 (1993).

Davis, R., and S. P. Thompson, ''Problem Solving Forum, How Rapid Depressurization Affects Linings in Pressurized Tanks and Pipelines,'' *J. of Protective Coatings & Linings*, **11**, 23 (1994).

Evans, R. B., III, G. M. Watson, and E. A. Mason, ''Gaseous Diffusion in Porous Media. II. Effect of Pressure Gradients,'' *J. Chem. Phys*., **36**, 1894 (1962).

Ferrero, M. A., and M. G. Chiovetta, ''Catalyst Fragmentation During Propylene Polymerisation, Part I. The Effects of Grain Size and Structure,'' *Poly. Eng. Sci*., **27**, 1436 (1987).

Krishna, R., ''A Simplified Procedure for the Solution of the Dusty Gas Model Equations for Steady-State Transport in Non-Reacting Systems,'' *Chem. Eng. J*., **35**, 75 (1987).

Krongelb, S., ''Environmental Effects on Chemically Vapor-Plated Dioxide,'' *J. Electrochem. Soc*., **6**, 251 (1968).

Mason, E. A., and A. P. Malinauskas, *Gas Transport in Porous Media: The Dusty Gas Model*, Elsevier, New York (1983).

Niegisch, W. D., S. T. Criafulli, T. S. Nagel, and B. E. Wagner, ''Characterisation Techniques for the Study of Silica Fragmentation with $MgCl_2$-Supported Ziegler-Natta Catalysts,'' *J. Appl. Poly. Sci*., **32**, 3047 (1994).

Perry, R. H., and D. W. Green, *Perry's Chemical Engineers' Handbook*, 6th ed., McGraw-Hill, New York (1984).

Sambuichi, M., H. Nakamura, K. Osasa, and F. M. Tiller, ''Theory of Batchwise Centrifugal Filtration,'' *AIChE J*., **33**, 109 (1987).

Saracco, G., G. F. Versteeg, and W. P. M. van Swaaij, ''Current Hurdles to the Success of High-Temperature Membrane Reactors,'' *J. Memb. Sci*., **95**, 105 (1994).

Strawbridge, A., and H. E. Evans, ''Mechanical Failure of Thin Brittle Coatings,'' *Eng. Failure Anal*., **2**, 85 (1995).

Tiller, F. M., and N. B. Hsyung, ''Unifying the Theory of Thickening, Filtration and Centrifugation,'' *Water Sci. Tech*., **28**, 1 (1993).

Westerterp, K. R., W. P. M. van Swaaij, and A. A. C. M. Beenackers, *Chemical Reactor Design and Operation*, Wiley, New York (1984).

Xia, J. L., B. L. Smith, and G. Yadigaroglu, ''A Simplified Model for Depressurization of Gas-Filled Pressure Vessels,'' *Int. Commun. Heat Mass Transfer*, **20**, 653 (1993).

Manuscript received June 17, 1998, and revision received Feb. 18, 1999.